ELSEVIER

Journal of Photochemistry and Photobiology A: Chemistry 149 (2002) 15–21

Journal of Photochemistry and Photobiology A:Chemistry

www.elsevier.com/locate/jphotochem

Photodissociation dynamics of *tert*-butyl hydroperoxide at 266 nm

Byung-Gyu Ryu [a], Chan Ryang Park [a], Yongsik Lee [b], Seung Keun Shin [c], Hong Lae Kim [c,*]

[a] *Department of Chemistry, College of Natural Sciences, Kookmin University, Seoul 136-702, South Korea*
[b] *Department of Chemistry, Kyunghee University, Suwon 449-701, South Korea*
[c] *Department of Chemistry, Kangwon National University, Chuncheon 200-701, South Korea*

Received 30 July 2001; received in revised form 10 December 2001; accepted 17 December 2001

Abstract

Photodissociation dynamics of *tert*-butyl hydroperoxide at 266 nm was investigated by measuring laser-induced fluorescence spectra of OH fragments. The OH fragments were produced exclusively in the $X^2\Pi$ states and spin–orbit ratios show approximately equal populations in the $^2\Pi_{3/2}$ and $^2\Pi_{1/2}$ states of OH. On the other hand, Λ-doublets favor the asymmetric A″ level for all measured values of N''. The distribution of total available energy among various degrees of freedom of products was found to be $f_{rot}(OH) = 0.06 \pm 0.01$, $f_{trans} = 0.51 \pm 0.05$, $f_{int}(t\text{-BuO}) = 0.43 \pm 0.06$, with negligible fraction of OH being produced in the vibrationally excited states. By analyzing Doppler profiles of the rotationally resolved OH spectra, vector correlations in the photodissociation of *tert*-butyl hydroperoxide were measured. The measured v–J correlation was positive and increased as N'' increased. From this observation and Λ-doublet preference, it was concluded that the parent torsional motion plays an important role in the rotational excitation of the OH fragment.

Keywords: *tert*-Butyl hydroperoxide; Laser-induced fluorescence spectra; Doppler profiles

1. Introduction

Studies of molecular photodissociation dynamics are of fundamental importance to investigate electronic structures of molecules because the process is governed by the excited state and potential energy surfaces along the reaction coordinate. The detailed dynamics of the process can be understood by measuring energies and certain vector properties of the system. These physical properties of the system can precisely be measured from optical spectra in favorable cases where the photofragments absorb and/or emit radiation in an easily accessible spectral region. The Doppler broadened absorption or emission spectra of the photofragments by polarized photolysis and probe light provide information on the energy distribution among various degrees of freedom of the fragments as well as directions of the transition dipole moment, recoil velocity and angular momenta of the fragments [1–3]. From the measurements, the excited state and the potential energy surfaces along the reaction coordinate can be identified.

Spectroscopic transitions in molecules to the repulsive part of the potential energy surface result in continuous spectra. One can theoretically determine the energies of the excited states and describe the nature of the transitions by ab initio calculations. When the dissociation starts from a part of the repulsive potential surface, the angular distribution of the fragments is especially important among many experimental observables in determining the nature of the excited state. Maximum absorption of the dissociating light by the molecule takes place when the transition dipole moment of the molecule lies along the electric vector of the linearly polarized dissociating light. Thus, the angular distribution of the recoiling fragments measured relative to the electric vector of the dissociating light in the laboratory frame reveals the direction of the transition dipole moment in the molecular frame. From the direction of the transition dipole moment, the symmetry of the excited state can be identified according to proper selection rules.

The Doppler profiles in polarized absorption and emission spectra of molecules have been thoroughly analyzed by Herschbach and coworkers [4,5]. The lineshapes of the spectra are determined by coupling of rotational and translational motion of the molecules. Thus, the Doppler broadened spectra of the photofragments provide relationships between the velocities and the rotational angular momenta of the fragments. The Doppler spectroscopic technique is limited by the resolution of the spectra. The translational energies of the fragments should be large enough to provide broad spectroscopic transitions, while the individual

* Corresponding author. Tel.: +82-33-250-8492; fax: +82-33-253-7582.
E-mail address: hlkim@cc.kangwon.ac.kr (H.L. Kim).

1010-6030/02/$ – see front matter
PII: S1010-6030(02)00005-9

rotational transition should also be resolved in the spectra under the given resolution. A commercial dye laser currently available typically provides 0.04 cm^{-1} bandwidth in the visible region, and various laser spectroscopic techniques such as laser-induced fluorescence (LIF) have been widely used to obtain the high resolution spectra of the photofragments.

Studies of the photodissociation of organic peroxides by irradiation of UV light have been reported for many years. In particular, the photodissociation of H_2O_2 in the first UV absorption band has been thoroughly studied [6–8]. The transition is assigned as $\sigma^* \leftarrow$ n whose transition dipole moment lies perpendicular to the O–O bond axis. The complete vector correlations have been measured, from which the detailed dynamics of the dissociation process at 266 nm have been analyzed. The photodissociation of $(CH_3)_3COOH$ is another good example of studying the dynamics by applying the Doppler spectroscopic technique. In addition, it is interesting to study the effect of alkyl substitution in H_2O_2 on the dissociation dynamics because the symmetry is lower and the substituted group is relatively heavy. $(CH_3)_3COOH$ is dissociated into *t*-butoxy (*t*-BuO) and OH radicals upon irradiation of the UV light. The photodissociation at 248 nm was studied by Simons and coworkers [9] in which slightly negative μ–v ($\beta = -0.2$) and slightly positive v–J correlation at high J have been observed. In the case of H_2O_2 at 266 nm, a negative μ–v correlation ($\beta = -1$) was reported [6]. The perpendicular transition in this spectral region results in the negative limiting value of the μ–v correlation in H_2O_2 but the relatively large *t*-BuO group affects the dynamics of the dissociation resulting in the smaller translational anisotropy parameter β in the case of $(CH_3)_3COOH$. At 193 nm, it was found that the transition leads to a mixture of the A and B states in $(CH_3)_3COOH$ and the dynamics was studied by measuring the vector correlations of the OH fragments [10]. The dissociation directly occurs from the repulsive A and B states and a large amount of the available energy has been found in the product translation. Crim and coworkers [11] studied the vibration-mediated photodissociation via the fifth overtone excitation of the OH stretching vibration of $(CH_3)_3COOH$. They found large internal excitation in the *t*-BuO group contrary to the direct dissociation from the repulsive state. Thus, it is also interesting to study the photodissociation dynamics of this molecule at lower photon energies by examining the substituent effect on energy disposal and the vector correlations.

The photodissociation dynamics of $(CH_3)_3COOH$ at 266 nm has been studied by measuring the LIF spectra of the OH fragments. By analyzing the Doppler profiles of the spectra, the energy distribution and the vector correlations of the fragments have been obtained.

2. Experiment

The experiment was performed in a flow cell with conventional pump-probe geometry. The cell was made of pyrex glass with crossed four arms and fused silica windows. Baffles were placed inside the arms to minimize scattered light. The cell was evacuated at a pressure of 10^{-4} Torr and gaseous sample was continuously flowed at a sample pressure of about 50 mTorr. The *tert*-butyl hydroperoxide was purchased from Aldrich (90% purity) and purified further before use by pumping through a glass sample cell until it reached a concentration of more than 95% in a standard mercury- and grease-free high-vacuum line.

The *tert*-butyl hydroperoxide was photodissociated by horizontally polarized light at 266 nm using an Nd:YAG laser (Specra Physiks GCR-150). Right after the photolysis laser pulse, horizontally polarized probe light was introduced into the cell, which was obtained from frequency doubling the output of a dye laser (Lumonics HD-500) pumped by the second harmonic of another Nd:YAG laser (Specra Physiks GCR-150). The time delay between the photolysis and probe laser beams was measured to be less than 10 ns. This delay time and 50 mTorr sample pressure should ensure nascent product energy distributions.

The frequency doubled tunable dye laser output probes the population of OH by exciting the (0, 0) and (1, 1) vibrational bands of the $A^2\Sigma \leftarrow X^2\Pi$ transition in the range 306–318 nm. The unresolved total fluorescence is subsequently detected from top of the cell at right angles to both the photolysis and probe laser beams with a high gain photomultiplier tube (Hamamatsu H3177) viewing through a broad-band ultraviolet filter consisting of UG11 glass and WG295. This combination of filters significantly attenuates the scattered photolysis light at 266 nm. The detected signal is then sampled with a boxcar averager and recorded in a laboratory computer system.

Conversion of the measured LIF signal to state-resolved OH population requires correction for variation in the intensities of both the photolysis and probe lasers as well as accurate values of the Einstein coefficients for stimulated absorption, *B*. Laser intensities were monitored and recorded simultaneously with the LIF signal during spectral scans. Tabulated values of *B*'s are used throughout. Under the present experimental conditions, electronic quenching of $OH(A^2\Sigma)$ by ambient gases does not affect the derived populations of even the lowest lying rotational levels [12,13]. The obtained populations need not be corrected for predissociation of the excited state because the highest rotational levels formed are well below the crossing of the $^4\Sigma^-$ state near 5300 cm^{-1} of $A^2\Sigma$, $v'' = 0$ [14]. The power of the probe laser light was kept as low as possible (typically 4 μJ/pulse, beam diameter 7 mm) to avoid saturation and to minimize the scattered radiation. The linearity of the LIF measurements was confirmed by comparing the relative intensities of the satellite and main branch transitions that probe the same level of OH: these were usually within a factor of 10% even though the *B* differs by factors of 2–6.

In order to measure the Doppler profiles of the spectra, several rotational transitions were probed under high resolution condition. The bandwidth of the probe laser light is

found to be 0.06 cm^{-1} in the visible, which was measured by the linewidth of the rotationally resolved gaseous I_2 LIF spectra at room temperature. The horizontally polarized photolysis and probe laser beams are collinearly counterpropagated or introduced at a right angle to the cell to obtain two different experimental geometries. The former geometry provides $\varepsilon_d \perp k_p$ and $\varepsilon_d \| \varepsilon_P$ while the latter geometry provides $\varepsilon_d \| k_p$ and $\varepsilon_d \perp \varepsilon_P$, where ε_d and ε_P are the directions of the electric vectors of the dissociating and probe laser lights and k_p the propagation direction of the probe light, respectively.

3. Results and analyses

The merged LIF spectra of the OH fragments produced from the photodissociation of $(CH_3)_3COOH$ is presented in Fig. 1.

Vibrational populations. Exclusive population of OH($X^2\Pi$, $v'' = 0$) can clearly be discerned from the merged spectra. The rotational transitions arising from the (1, 1) band region (312–318 nm) have been measured but no appreciable intensities were observed. Individual rotational transitions in the (0, 0) band of the A–X transition are resolved and assigned according to Luque and Crosley [15]. Conversion of the spectrum to relative micropopulations (the state populations divided by their rotational degeneracy, $2J'' + 1$) yields the distributions displayed in Fig. 2.

Rotational populations. As shown in Fig. 2, the overall rotational distribution cannot be characterized by a single rotational temperature, although the distribution at $N'' > 6$ roughly follows a Boltzmann form with a rotational temperature of about 1200 K. From the observed distributions for each branch, the average rotational energy of the OH products was calculated to be about $1400 \pm 100\ cm^{-1}$.

Electronic populations. Spin–orbit coupling causes the existence of two fine structure states, f_1 and f_2, that correspond to $X^2\Pi_{1/2}$ and $X^2\Pi_{3/2}$, respectively. Analysis of the spectra reveals that there is no significant difference in the fine structure state micropopulations summed over all the accessible rotational levels ($P(^2\Pi_{1/2})/P(^2\Pi_{3/2}) = 1.08$ for OH($X^2\Pi$, $v'' = 0$)). This should be contrasted to the previously reported preferential population of the lower-lying f_1 state following the formation of OH in the bimolecular reaction of $O(^3P_J)$ with hydrocarbons, a reaction that is known to proceed via a direct abstraction mechanism [16].

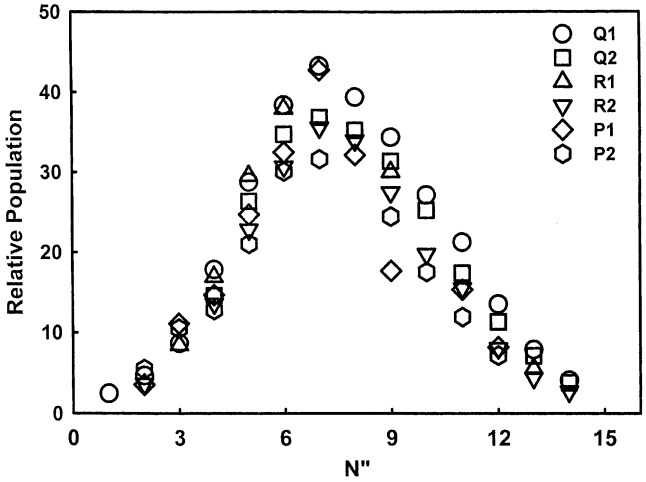

Fig. 2. Rotational population distribution of OH obtained from the spectra in Fig. 1.

Coupling of orbital and rotational angular momenta produces two Λ-doublet fine structure states, $\Pi^+(A')$ and $\Pi^-(A'')$, the former corresponding, in the limit of high rotational states, to orientation of the half-filled p_π orbital in the plane of molecular rotation, the latter to orientation at 90° to that plane. The relative populations of OH produced in the $\Pi^+(A')$ and $\Pi^-(A'')$ states, probed by P/R and Q branches, respectively, shows preferential population of the $\Pi^-(A'')$ state (Fig. 3), thereby providing some

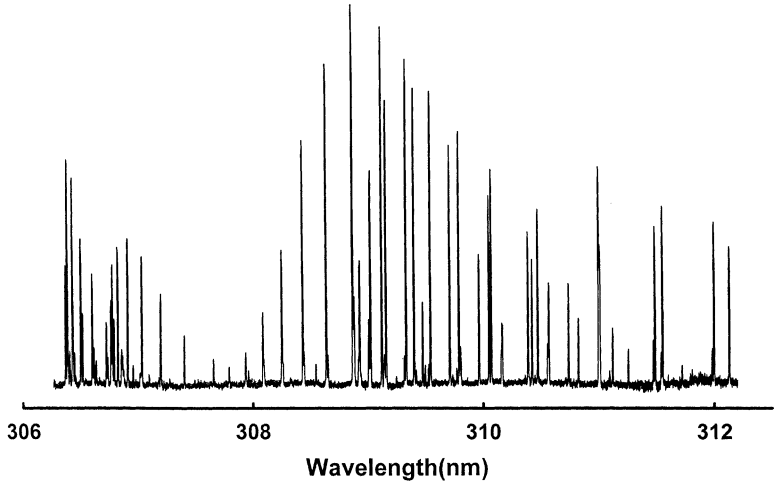

Fig. 1. Laser-induced fluorescence excitation spectra of OH produced from photodissociation of $(CH_3)_3COOH$ at 266 nm employing the A ← X transition.

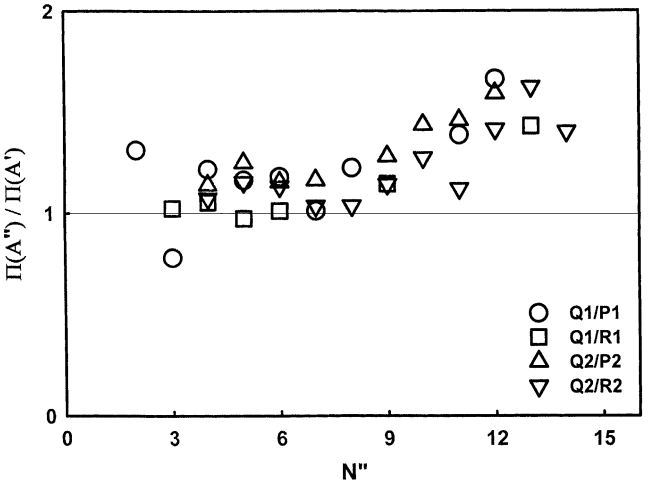

Fig. 3. Λ-Doublet distribution of OH produced from photodissociation of $(CH_3)_3COOH$ at 266 nm.

support for a mechanism in which the OH product is formed following an orienting dissociation, i.e., during the course of $(CH_3)_3COOH^{\dagger}$ fragmentation.

Vector correlations. Correlations of rotation with translational motion have been thoroughly analyzed by Dixon [17] and the anisotropy is defined by a number of bipolar moments of the translational and rotational angular distributions. The Doppler-broadened line shape in the LIF spectra of the photofragments depends on the rotational alignments, the polarization of the photolysis and probe lights, the excitation–detection geometries, and the branch of the rotational transitions probed. The generalized line shape functions are then given by

$$g(\chi_D) = \frac{1}{2\nu_D}[g_0 + g_2 P_2(\chi_D) + g_4 P_4(\chi_D) + g_6 P_6(\chi_D)] \quad (1)$$

where χ_D and ν_D are the relative and the maximum Doppler shift, respectively, and P's are the even-order Legendre polynomials. The Legendre polynomials of the fourth- and sixth-order are often neglected since the contribution of these high order terms to the Doppler profiles are small compared to the experimental errors. The multipliers, g's in Eq. (1), are the linear combination of the bipolar moments, β_0^k, which are given by

$$g_0 = b_0 + b_1\beta_0^2(02) \quad (2)$$

$$g_2 = b_2\beta_0^2(20) + b_3\beta_0^0(22) + b_4\beta_0^2(22) \quad (3)$$

where b's can be calculated from the excitation–detection geometries and the angular momentum coupling factors defined by Dixon [17]. In this experiment, the two different excitation–detection geometries described in Section 2 have been employed, and the corresponding b values have been obtained for the different rotational branch transitions [18]. The bipolar moments $\beta_0^2(02)$, $\beta_0^2(20)$, $\beta_0^0(22)$, $\beta_0^2(22)$ represent the rotational alignment, $\beta_{\mu J}$, translational anisotropy, $\beta_{\mu v}(= 2\beta_0^2(20))$, v–J, and μ–v–J photofragment vector correlations, respectively. The experimental Doppler profiles are fitted by the equation

$$g(\chi_D) = \frac{1}{2\nu_D}[1 + \beta_{eff} P_2(\theta) P_2(\chi_D)] \quad (4)$$

where θ is the angle between the recoil velocity and the probe direction and

$$\beta_{eff} = \frac{b_2\beta_0^2(20) + b_3\beta_0^0(22) + b_4\beta_0^2(22)}{g_0 P_2(\theta)} \quad (5)$$

From the least-squares fit of the observed profiles to Eq. (5), the four bipolar moments can be calculated by solving the linear equations.

The Doppler resolved spectra have been measured for the P1 and Q1, or R1 and Q1 rotational branch transitions for the rotational quantum numbers $N'' = 4$, 5, 6, 7, 9, 10, 11, 12, 13 which are well separated from other transitions. In Fig. 4, typical Doppler-broadened LIF spectra for $N'' = 11$ are presented. Since the *t*-BuO fragments should have internal energy distributions, the OH fragments should have corresponding speed distributions. Since the internal energy distributions of the *t*-BuO fragments have not been measured in this experiment, the measured profiles have been fitted assuming Gaussian speed distribution with various widths. In order to find the best fits, the following procedures were employed. First, the best fit was found to the observed profile of one rotational branch transition varying β_{eff}, the average speed, and the width of the speed distribution. The measured average speed and the width for the

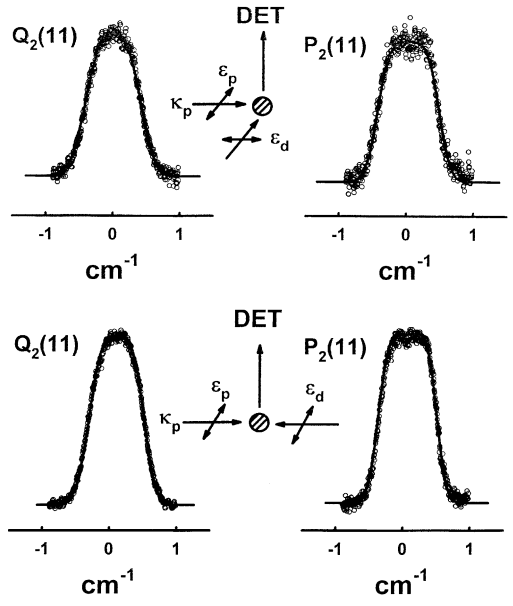

Fig. 4. Rotationally resolved Doppler profiles in the spectra of OH obtained from different branch transitions under different excitation–detection geometries.

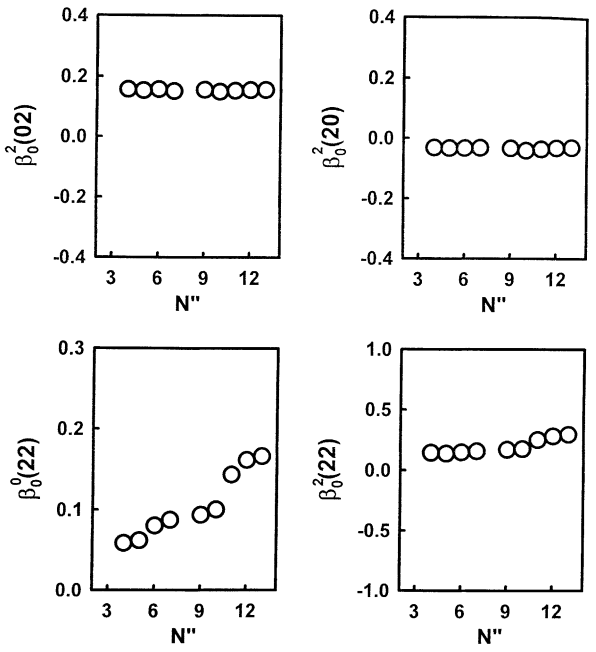

Fig. 5. Vector correlations in the photodissociation of $(CH_3)_3COOH$ at 266 nm obtained from the Doppler profiles in the spectra of OH.

best fit are 3800 and 200 ms^{-1} for $N'' = 11$, respectively. Then, for the profiles of the different rotational branch transitions under different experimental geometries at the same N'', the best fit was obtained by just varying β_{eff}. From the measured β_{eff}'s for the same N'', the bipolar moments are calculated by solving the linear equations. The calculated bipolar moments for different N's are presented in Fig. 5. In the figure, the negative translational anisotropy ($\beta_{\mu v} = -0.1$) indicates the OH fragments should be essentially ejected perpendicular to the transition dipole moment of the parent molecule, although the value is far from the limiting value of -1. The positive increasing v–J correlation with increasing N'' implies more parallel orientation of the rotational angular momentum J_{OH} to the recoil velocity v_{OH} (out-of-plane dissociation). In addition, slightly positive μ–v and positive μ–v–J correlations were also observed.

4. Discussion

The UV Spectrum of *tert*-butyl hydroperoxide shows continuous absorption starting from around 300 nm due to the transitions from the ground state to repulsive A, B, and C states. The absorption at 266 nm could be identified as the $n \rightarrow \sigma^*$ transition along the O–O bond to the lowest repulsive A state. Thus, similar to the 248 nm case, the photodissociation dynamics of *tert*-butyl hydroperoxide can be understood as the electronic transition at 266 nm to this repulsive surface results in the direct, impulsive dissociation. In H_2O_2, the direction of the transition dipole moment of the lowest electronic transition to the repulsive A state is perpendicular to the dissociating O–O bond (perpendicular transition). Although the *t*-butyl substitution to H_2O_2 lowers the overall symmetry of the parent molecule and hence the direction of the transition dipole moment cannot be clearly identified, the transition at this wavelength could be still assumed essentially perpendicular. The measured negative translational anisotropy parameter of -0.1 is the result of this perpendicular transition, though the limiting value is -1 for the pure perpendicular transition. In fact, the translational anisotropy parameter of -1 was observed in the dissociation of H_2O_2 from the repulsive A state at 266 nm [6]. The deviation of the translational anisotropy parameter from the limiting value might be due to molecular rotation of the parent molecule during the dissociation and/or to some dynamical effects. However, judging from the repulsive nature of the dissociating surface and the slow rotational period of the parent molecule on the order of picoseconds, it is unlikely that the molecular rotation reduces the translational anisotropy. Thus, as Simons and coworkers pointed out [9], it is suggested that the bending torque at the impulse would deflect the fragment OH out of the recoil direction, which will substantially reduce the translational anisotropy.

The dissociation energy of *tert*-butyl hydroperoxide into *t*-BuO and OH is 37.6 kcal/mol. Then, the available energy, which can be distributed among the fragments from the photodissociation at 266 nm is 25,040 cm^{-1} and the measured fractions of the available energy in the products are listed in Table 1. The measured energy partitioning in the fragments is well explained by the impulsive dissociation model, which assumes direct and fast dissociation [19]. In the model, the initial excitation is expected to turn on the impulsive force between the departing O–O atoms. The linear momentum of the atoms is then transferred to the fragments and the average translational and internal energies of the fragments are calculated based upon the momentum and energy conservation. Therefore, the translational and rotational energy of the OH fragment can be calculated by the

Table 1
Fraction of the available energy distributed among the products produced from the photodissociation of $(CH_3)_3COOH$ at 266 nm

E_{av} (cm^{-1})	$\langle f_{trans} \rangle$	$\langle f_{rot}(OH) \rangle$	$\langle f_{vib}(OH) \rangle$	$\langle f_{int}((CH_3)_3CO) \rangle$
25,040[a]	0.51 ± 0.05	0.06 ± 0.01	<0.01[b]	0.43 ± 0.06
Impulsive model	0.54	0.03	0.001	

[a] $E_{av} = h\nu + E_{int}((CH_3)_3COOH \text{ at } 300\,K) - D_0((CH_3)_3CO\text{–}OH)$.
[b] Approximated from the noise in the spectra.

following equations

$$E_{\text{trans}}(\text{OH}) = \frac{m(t\text{-BuO})}{M}\frac{\mu(\text{O–O})}{\mu(t\text{-BuO–OH})}E_{\text{av}},$$

$$E_{\text{rot}}(\text{OH}) = \left(\frac{m_{\text{H}}}{m_{\text{O}} + m_{\text{H}}}\right)^2 \sin^2\chi\, E_{\text{av}}$$

where M is the mass of the parent molecule, μ's the reduced masses and χ the angle $\angle$(OOH). The measured energy distribution implies that the dissociation is direct and fast from the repulsive surfaces as mentioned above. In the impulsive model calculation, it was assumed that the geometry of *tert*-butyl hydroperoxide in the excited state would be the same as the geometry in the ground state. However, a recent quantum dynamical calculation of the photodissociation of H_2O_2 shows that the rotational population distribution of the OH fragment should be Gaussian-like with a tail at high N due to bending and torsional couplings [20,21]. If more torsional couplings are taken into account, the distribution shows more tailing to the high N side. The ab initio calculations of the equilibrium geometry of H_2O_2 indicate the dihedral angle of 120° at the *trans* planar geometry and the barrier for corresponding *cis–trans* configuration change is 386 cm^{-1} [22]. The alkyl substitution slightly opens the dihedral angle in CH_3OOH and greatly reduces the barrier ($\sim$80 cm^{-1}). Assuming the similar trend in *t*-butyl substitution, the barrier is expected to be much lower than the zero point energy of the OH torsional motion. Thus, the wide angle torsional motion of the parent molecule is likely transformed to the fragment OH rotational motion upon dissociation and the rotational population distribution observed in this experiment reflects the importance of the parent torsional motion, especially at high N. The fact that the parent torsional motion plays an important role in the OH fragment rotation is ascertained by the positive v–J vector correlation measured in this experiment.

Coupling between rotation and translational motion can be analyzed by the shape of the Doppler profiles of the spectra of the OH fragment. Since the v–J correlation is developed at the moment of dissociation, it can be observed even in the isotropic dissociation. If the source of the fragment OH rotation is solely the bending torque or the impulsive force, the rotational angular momentum should be aligned perpendicular to the recoil direction. In this case, the negative v–J correlation is expected. However, if the parent torsional motion is the source of the OH rotation, the rotational angular momentum should be aligned parallel to the recoil direction and hence the positive v–J correlation would be observed. The v–J correlation measured in this experiment is positive and increases as N increases, implying again that the parent torsional motion plays the important role in the fragment OH rotation.

In a diatomic molecule with a singly occupied p_π orbital such as OH produced in this experiment, coupling between the electronic angular momentum and nuclear rotation splits the two degenerate states of $\Lambda = \pm 1$, the orbital angular momentum projection to the internuclear axis [23]. In the limit of high rotation, the p_π orbital is approximated as a lobe aligned perpendicular to the plane of rotation (Π^-, the lower Λ state) or a lobe in the plane of rotation (Π^+, the upper Λ state). According to the parity selection rule, the Q-branch rotational transition is induced from the Π^- state while the R- and P-branch transitions are induced from the Π^+ state in the electronic transition. Thus, the specific Λ-doublet population can be experimentally measured in the spectra. The distribution between the two Λ-doublet states of OH produced in the photodissociation depends upon the correlation on the p_π orbital of the OH fragment with the orbitals of the parent molecule and how the p_π orbital is generated upon dissociation, that is the mechanism of the dissociation process. The measured Λ-doublet distribution shows a propensity in the Π^- state and the propensity is increased as N is increased indicating the unpaired p_π orbital of the OH fragment is more aligned perpendicular to the plane of rotation. The higher propensity in the Π^- state of OH recoiling with higher rotational angular momentum indicates that the p_π orbital lobe of the OH fragment conserves some of the orientations of the corresponding p_π orbital in the excited parent molecule just before dissociation and reflects the importance of the angular motion such as torsion on the excited surfaces.

In summary, the electronic transition at 266 nm leads the molecule to the repulsive A state in *tert*-butyl hydroperoxide, from which the direct and impulsive dissociation takes place. The experimental results show that the parent torsional motion plays an important role in the rotation of the OH fragments.

Acknowledgements

This work was financially supported by the Korea Science and Engineering Foundation.

References

[1] G.E. Hall, P.L. Houston, Ann. Rev. Phys. Chem. 375 (1989) 40.
[2] M.N.R. Ashfold, J.E. Baggott (Eds.), Molecular Photodissociation Dynamics, Royal Society of Chemistry, London, 1987.
[3] J.P. Simons, J. Phys. Chem. 91 (1987) 5378.
[4] R.N. Zare, D.R. Herschbach, Proc. IEEE 51 (1963) 173.
[5] C.H. Greene, R.N. Zare, Ann. Rev. Phys. Chem. 33 (1982) 119.
[6] K.-H. Gericke, S. Klee, H.J. Comes, R.N. Dixon, J. Chem. Phys. 85 (1986) 4463.
[7] G. Ondrey, N. van Veen, R. Bersohn, J. Chem. Phys. 78 (1983) 3732.
[8] A.U. Grunewald, K.-H. Gericke, H.J. Comes, J. Chem. Phys. 87 (1987) 5709.
[9] J. August, M. Brouard, M.P. Docker, C.J. Milne, J.P. Simons, R. Lavi, S. Rosenwaks, D. Schwartz-Lavi, J. Phys. Chem. 92 (1988) 5485.
[10] S.K. Shin, H.L. Kim, C.R. Park, J. Phys. Chem. A 103 (1999) 4150.
[11] M.D. Likar, J.E. Baggott, A. Sinha, T.M. Ticich, R.L. Vander Wal, F.F. Crim, J. Chem. Soc., Faraday Trans. 84 (1988) 1483.
[12] R.A. Copland, D.R. Crosley, Chem. Phys. Lett. 107 (1984) 295.
[13] R.A. Copland, M.J. Dyer, D.R. Crosley, J. Chem. Phys. 82 (1985) 4022.

[14] R.A. Sutherland, R.A. Anderson, J. Chem. Phys. 58 (1973) 1226.
[15] J. Luque, D.R. Crosley, J. Chem. Phys. 109 (1998) 439.
[16] P. Anderson, A.C. Luntz, J. Chem. Phys. 72 (1980) 5842.
[17] R.N. Dixon, J. Chem. Phys. 85 (1986) 1866.
[18] S.J. Baek, C.R. Park, H.L. Kim, J. Photochem. Photobiol. A 104 (1997) 13.
[19] G.E. Busch, K.R. Wilson, J. Chem. Phys. 56 (1972) 3626.
[20] R. Bersohn, M. Shapiro, J. Chem. Phys. 85 (1986) 1396.
[21] D.H. Zhang, J.Z.H. Zhang, J. Chem. Phys. 98 (1992) 6276.
[22] R.A. Bair, W.A. Goddard III, J. Am. Chem. Soc. 104 (1982) 2719.
[23] I. Hanazaki, Chem. Phys. Lett. 201 (1993) 301.